2013-12-10

RF Transport Electromagnetic Properties of Graphene from DC to 110 MHz

Awan, SA

10.1049/iet-cds.2014.0204
Measurement, Science and Technology
Institute of Physics

RF Transport Electromagnetic Properties of Graphene from DC to 110 MHz

Shakil A Awan[1], Genhua Pan[1], Laith M Al Taan[1,2] and Bing Li[1]

[1]School of Computing and Mathematics, Faculty of Science and Environment, University of Plymouth, Drake Circus, Plymouth, PL4 8AA, UK

[2]Department of Physics, College of Science, University of Mosul, Iraq

E-mail: shakil.awan@plymouth.ac.uk

Abstract

The paper describes measurement of RF transport electromagnetic properties of CVD graphene over the DC to 110 MHz frequency range at room temperature. Graphene on Si/SiO_2 substrate was mounted in a shielded four terminal-pair (4TP) adaptor which enabled direct connection to a calibrated precision impedance analyser for measurements. Good agreement is observed for the DC four-probe resistance and the 4TP resistance at 40 Hz, both yielding $R \approx 104\ \Omega$. In general the apparent graphene channel electromagnetic properties are found to be strongly influenced by quantum contact effects, such as resistance and capacitance, particularly at DC and low frequencies $f < 1$ MHz. A phenomenological lumped-parameter equivalent circuit model is presented which matches the frequency response of the graphene 4TP impedance device over approximately seven decades of the frequency range of the applied transport alternating current. Based on this model, the intrinsic graphene channel resistance is found to be $R_G = 2.2\ \Omega$ or sheet resistance of $3.85\ \Omega / \square$, which is frequency independent, with each contact impedance being $R_C = 51.6\ \Omega$ and $C_C = 1.2$ nF. These results suggest that our RF 4TP method may be more accurate and reliable than the conventional DC four-probe method for measuring the intrinsic sheet resistance of single-atom thick materials such as graphene. This may be significant for the production and optimisation of graphene for solar-cells and touch-screen displays where sheet resistance (combined with its optical transparency) figures-of-merit play an important role, particularly in comparison with the values of the current material of choice, indium tin oxide (ITO), for such applications.

Keywords: Graphene, 2D materials, radio-frequency, electronics, 2DEG, nanoelectronics, nanofabrication, impedance measurements

1. Introduction

Graphene, an atomically thin two-dimensional allotrope of carbon [1], has recently been found to show a number of physical properties, such as high carrier mobility [1-3], ambipolar field-effect [1-5], high current carrying capacity [4] and thermal conductivity [6], which are promising for numerous applications, particularly for nanoelectronics and optoelectronics [7-11]. To date, majority of the effort on nanoelectronics has been focused on DC transport properties of graphene, based on field-effect transistors [12-15], and optical properties of mono and multilayer graphene [16-22]. Although graphene is a promising material for high-frequency applications such as RF transistors [23-26], low-noise amplifiers [27], mixers [28] and frequency doublers [28,29], only a few investigations into the high-frequency transport properties of graphene have been reported [30-33]. Furthermore, given that graphene serves as the channel material in radio-frequency (RF) transistors, significant effort has been devoted to characterization and modeling of RF transistors [24-26, 34-37], rather than characterizing the building block material itself at RF [38,39]. Here, we report on the RF electromagnetic transport properties of monolayer chemical vapour deposition (CVD) graphene carrying transport direct current (DC) and alternating current (AC) with frequencies ranging from 40 Hz to 110 MHz.

For some electronic applications of graphene there are three regions of the electromagnetic spectrum which are of key importance for characterising the material properties; DC, RF (covering power frequencies to 300 MHz) and microwaves (covering 0.3-300 GHz). Measurements of graphene at DC are potentially the most precise and relatively easy to implement (such as 2-probe and 4-probe) under variety of applied conditions, such as temperature, magnetic field etc. for elucidating the material or

device properties [1-5]. However, DC measurements are limited in providing any information on the dynamic properties of a material or device. In particular, quantum contact effects at DC often mask the intrinsic properties which can readily be extracted using RF or microwave measurements. For the latter there are two types of workhorse instruments which enable precise and traceable measurements; impedance analysers (IAs) for RF measurements and vector network analysers (VNAs) for microwave measurements. Although VNAs offer broadband measurements up to 110 GHz, their accuracy is limited and depending on the frequency range of operation, it can vary from 1-10%. In contrast, the IAs are limited in frequency range, typically 40 Hz to 110 MHz, but can be highly precise and accurate if they are first calibrated using impedance standards of known frequency response [40,41]. Impedance analysers (sometimes also referred to as inductance-capacitance-resistance, or LCR meters) are in widespread use in industry ranging from electronic component manufacturers and telecommunications to biomedical and defence as well as research and development laboratories to academia. They are regarded as workhorse instruments because of their wide range of impedance measurement capabilities, covering LCR parameters in the 40 Hz to 110 MHz part of the electromagnetic spectrum. High accuracy impedance analysers are also useful in metrology laboratories for comparison of impedance standards, such as inductance, capacitance and resistance standards [42]. They are particularly useful for making one-to-one comparison measurements of standards, with nominally the same impedance, where substitution techniques [43] may be applied to reduce the measurement uncertainty of a device-under-test (DUT).

Here, we demonstrate that using a precision four terminal-pair (4TP) impedance analyser with a high-frequency calculable resistance standard (HF-CRS) to calibrate the IA, the intrinsic properties of CVD graphene can be extracted accurately up to 110 MHz for the first time. The results could impact future applications of graphene in electronic devices by enabling optimisation of the production processes, device design, theory, modelling and indeed accurate characterisation. In addition, our results also demonstrate that the conventional DC four-probe (4P) sheet resistance measurement method [44] may not be appropriate for accurately determining the intrinsic properties of graphene due to the presence of quantum contact resistance which is always present between a metal and a single-atom thick material. This may be important in applications such as solar cells, touch-screen displays etc. where the combined properties of a material's sheet resistance and optical transparency are the two key figures of merit which require optimisation [11].

2. Design and Fabrication of the Graphene 4TP Impedance Device

Figure 1 shows the design outline and fabricated graphene four terminal-pair (G-4TP) impedance device. Monolayer graphene, confirmed using Raman spectroscopy [45], was placed on a high resistivity (10 kΩ-cm) Si/SiO_2 substrate to reduce the effects of parasitic impedances and substrate losses at high-frequencies. The length and width of the graphene channel is ~ 35 μm between the source-drain or current contacts. Three narrower potential contacts are also patterned on both sides of the graphene channel using photolithography, as shown in Fig. 1. All contacts consist of a 2nm Cr adhesion layer and 80 nm thick Au layer. For a 4TP measurement only potential contacts 1 and 4 as well as the current contacts are used, whilst the other potential contacts remained open circuited.

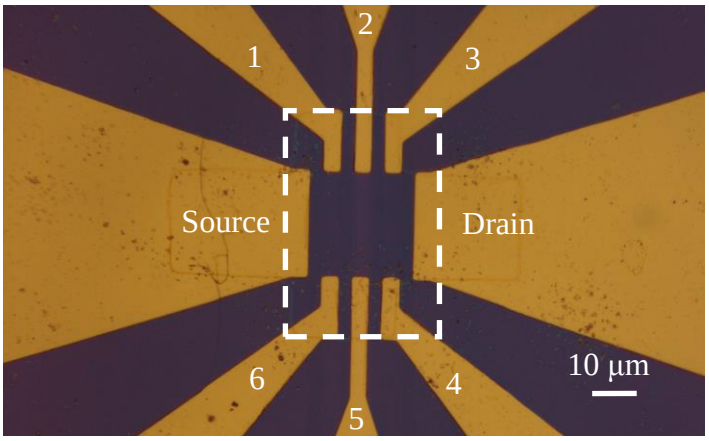

Figure 1. Graphene 4TP impedance device on a Si/SiO_2 substrate for measurements at frequencies up to 110 MHz. The dashed outline illustrates location of CVD graphene.

3. DC Characterisation of the Graphene 4TP Impedance Device

Figure 2 shows the two-probe (2P) and four-probe (4P) DC *IV*-characteristics of the graphene 4TP impedance device. As expected, the I_{SD} versus V_{SD} is linear and the corresponding 2P resistance between the current contacts is found to be $R_{2P} \approx 378\ \Omega$. Similarly, the 4P resistance between the potential contacts (1 and 4), with a channel length of $l = 20$ μm and width $w = 35$ μm, is found to be $R_{4P} \approx 104\ \Omega$, at zero back-gate potential. The corresponding sheet resistance (in units of Ω / □) for a

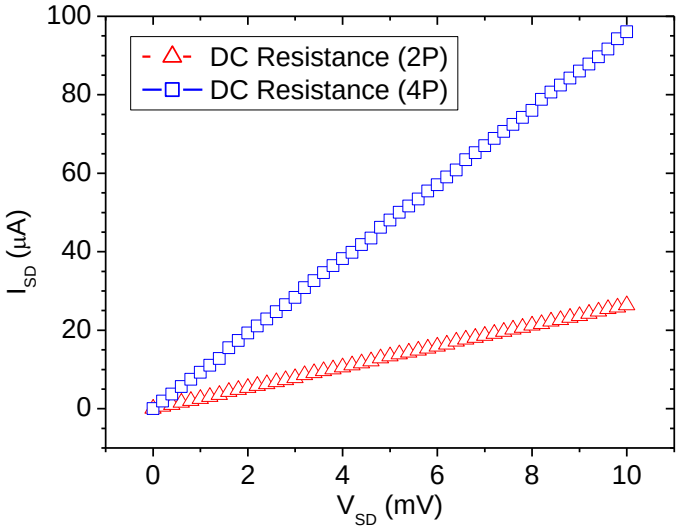

Figure 2. DC two-probe (source-drain)) and four-probe (using potential contacts 1 and 4) *IV*-characteristics of the graphene 4TP impedance device. The 2P resistance is found to be ≈ 378 Ω whereas the 4P resistance is found to be ≈ 104 Ω, at zero back-gate potential.

two-dimensional material [44] is given by $R_S = (w/l) \cdot R_{4P}$ and for our device we find $R_S^{DC} \approx 182\Omega/\square$ at DC and a channel conductivity of $\sigma = (R_S)^{-1} \approx 142e^2/h$, where e is the electronic charge and h the Planck's constant. After the DC *IV*-characterisation, the G-4TP impedance device was mounted in a shielded adaptor (illustrated in Fig. 3(a)) to enable direct connection with an Agilent 4294A four terminal-pair impedance analyser for measurements up to 110 MHz. The direct connection of the graphene device to the IA is important for two key reasons; firstly this avoids use of coaxial cables to connect the device to IA thereby enabling accurate measurements which would otherwise require cable corrections [43], and secondly the IA is calibrated using a HF-CRS which also makes direct 4TP connections with the IA (further details of this are given in Section 4.0). As the 4TP adaptor requires high and low current contacts and two high and low potential contacts (1 and 4, respectively), the remaining potential contacts were left open circuited during RF measurements. At microwave frequencies these open circuit leads may give rise to resonances and parasitic effects, however at the lower ~100 MHz frequencies, these are found to have negligible effect on the measured transport properties of our graphene 4TP impedance device. The definition of a 4TP impedance was first devised by Cutkosky in 1964 [46]. It is possible to rewrite the 4TP definition for a general linear network as shown in Fig. 3(*a*), such that

$$\begin{bmatrix} V_1 \\ V_2 \\ V_3 \\ V_4 \end{bmatrix} = \begin{bmatrix} Z_{11} & Z_{12} & Z_{13} & Z_{14} \\ Z_{21} & Z_{22} & Z_{23} & Z_{24} \\ Z_{31} & Z_{32} & Z_{33} & Z_{34} \\ Z_{41} & Z_{42} & Z_{43} & Z_{44} \end{bmatrix} \cdot \begin{bmatrix} I_1 \\ I_2 \\ I_3 \\ I_4 \end{bmatrix} \qquad (1)$$

where V and I are the voltages and currents at the four respective ports and $Z_{ij} \equiv V_i/I_j$, so that $I_{j \neq k} = 0$ with $1 \leq (i, j, k) \leq 4$, such that for a linear reciprocal 4TP network $Z_{ij} = Z_{ji}$ are the two terminal-pair (2TP) impedance parmeters. Thus, the four terminal-pair impedance is given by :

$$Z_{4TP} = \left.\frac{V_2}{I_4}\right|_{I_2=I_3=V_3=0} \tag{2}$$

Also shown in Fig. 3(b) is the RF equivalent circuit phenomenological lumped-parameter model of the graphene 4TP impedance device. The significance and suitability of this circuit model for the G-4TP impedance device is discussed in Section 5.0.

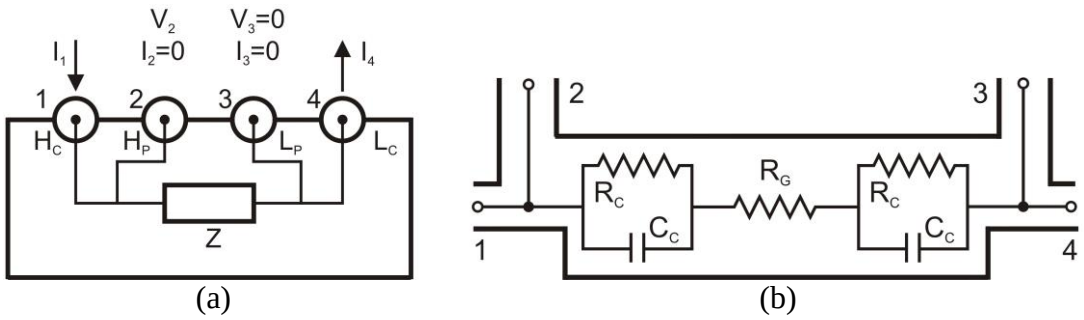

Figure 3. Four terminal-pair definition of impedance *Z* or device-under-test mounted in a shielded adaptor (a) and the RF equivalent circuit phenomenological lumped-parameter model of the graphene 4TP impedance device consisting of contact impedances and channel resistance R_G (b). Ports labelled 1-4 in both diagrams are often also referred to as high-current (H_C), high-potential (H_P), low-potential (L_P) and low-current (L_C), respectively.

4. Calibration of the 4TP Impedance Analyser

The IA was first calibrated using one of our 100 Ω high-frequency calculable resistance standards [40], since the G-4TP impedance device had a DC value of $R_{4P} \approx 104\ \Omega$. The IA instruments use number of range resistors internally, such as 100 Ω and 1 kΩ etc., against which a DUT is measured in a comparison bridge. It is these range resistors which require calibration against a standard of known frequency response over the broad frequency range of the IA. The schematic layout of the 4TP coaxial HF-CRS is shown in Fig. 4 [40]. These types of standards were specifically developed to calibrate and to verify the correct operation of IAs and LCR meters from DC to 110 MHz (and to enable robust comparison of such instruments from different commercial suppliers). The frequency response of the HF-CRS can be calculated from first principles based on Maxwell's equations and the full analytical derivation of the expressions for frequency-dependent resistance, inductance and capacitance are given in [43]. The 4TP impedance of the standard is given by:

$$Z_{4TP}(\omega) = \frac{R + i\omega\left[L\left(1-\omega^2 LC\right) - CR^2\right]}{1+\omega^2\left[C^2R^2 - 2LC + \omega^2L^2C^2\right]} \tag{3}$$

where R is the measured DC resistance of the standard, $\omega = 2\pi f$, inductance $L = 0.19$ μH and capacitance $C = 2.1$ pF are the calculated values of the standard based on the dimensions and geometry of the standard. Figure 5 shows the measured apparent resistance and reactance of the 100 Ω HF-CRS, using Agilent 4294A, up to 110 MHz. Good agreement is observed between the measured and calculated frequency response of the HF-CRS, for both resistance and reactance, up to 110 MHz, confirming accurate calibration of the range resistors (to ~1% for $f < 100$ MHz, and ~5% for $f > 100$ MHz). An instrument artefact occurs at 15 MHz, as shown in the measured apparent resistance and reactance data. This is due to the instrument switching between its two internal bridge measurement systems (which the manufacturer refers to as auto-balancing and I-V bridges) covering the frequency ranges above and below 15 MHz, respectively.

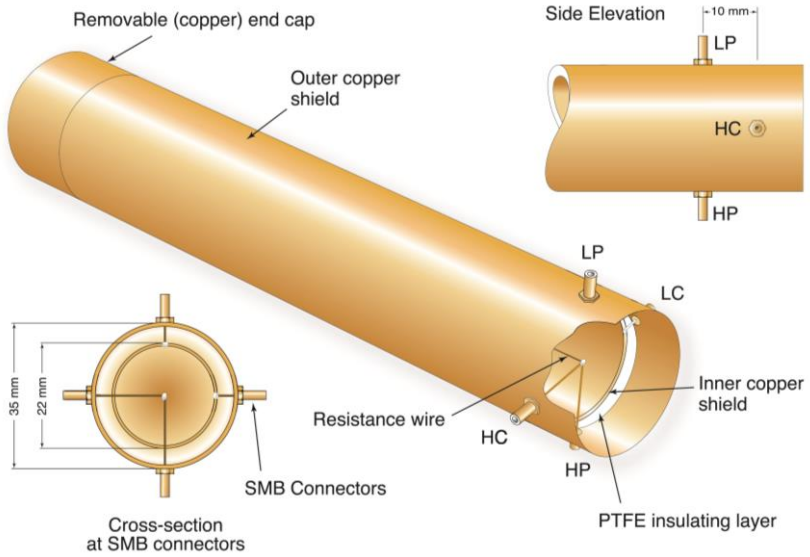

Figure 4. Schematic of the coaxial 4TP high-frequency calculable resistance standard (with permission from *IEEE* [40]).

5. Characterisation of the CVD Graphene 4TP Impedance Device

Figure 6 shows the measured and modelled frequency response of the graphene 4TP impedance device from 40 Hz to 110 MHz (with zero back-gate potential) at room temperature. At 40 Hz the measured 4TP resistance of ≈ 105 Ω is in good agreement with the 4P DC measured resistance of ≈ 104 Ω. At higher-frequencies, the apparent resistance and reactance show good agreement with the model of Fig. 3(b), using least-squares fitting parameters R_G = 2.2 Ω, R_C = 51.6 Ω and C_C = 1.2 nF. The measurement results shown in Fig. 6 and the equivalent circuit model of Fig. 3(b) suggest that any inductive or capacitive components for the graphene channel are negligible for this device of l = 20 μm channel length and upper operational frequency of 110 MHz. It is worth noting that the intrinsic resistance, although its present from DC to 110 MHz, it can only be observed for f > 1MHz which is also simultaneously accompanied by the apparent reactance tending to approximately zero Ohms. The relatively small differences between the measured apparent resistance and reactance with the simulated values, based on the model of Fig. 3(b), may be due to the slight differences between the contact impedances at the potential contacts (due to their small but finite width of ~ 5 μm). The relatively complex frequency-dependent response of G-4TP in Fig. 6, for both resistance and

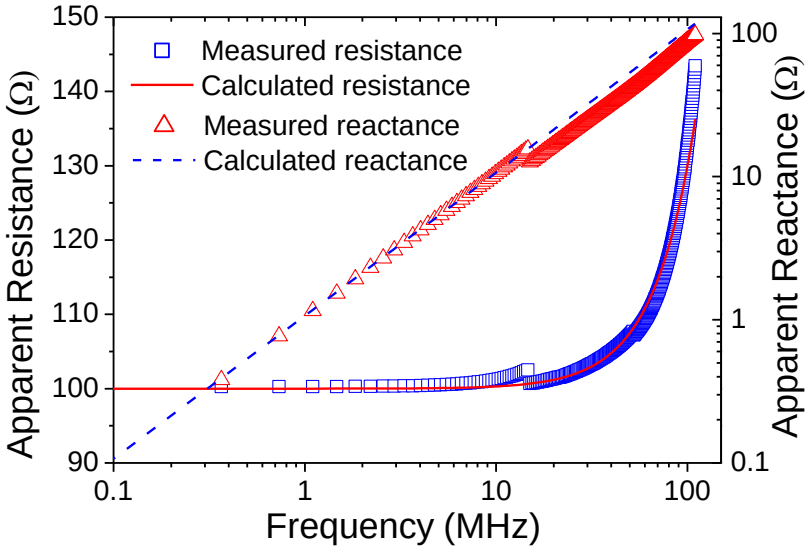

Figure 5. Measurement of the 4TP HF-CRS on Agilent 4294A at frequencies up to 110 MHz. The solid and dashed lines are the calculated response of the HF-CRS based on equation (3) [43].

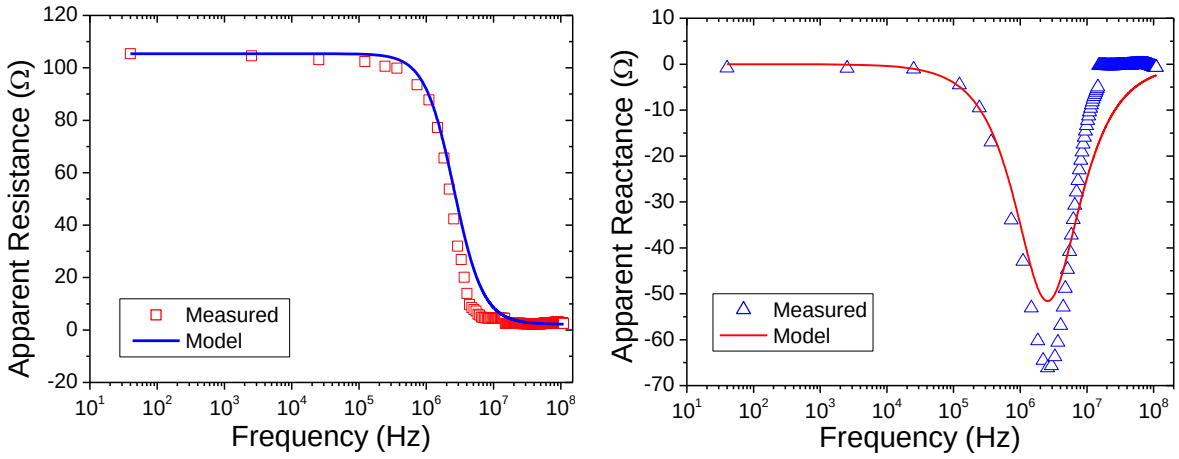

Figure 6. Measured and modelled apparent resistance and reactance of the graphene 4TP impedance device from 40 Hz to 110 MHz. The solid line is the model of Fig. 3(b) with fitting parameters R_G = 2.2 Ω, R_C = 51.6 Ω and C_C = 1.2 nF.

reactance, demonstrates that the quantum contact resistance and capacitance have a strong influence on the apparent electromagnetic behaviour of the graphene channel. In addition, the DC and low-frequency (f < 1MHz) measurements, suggest approximately two orders-of-magnitude higher *apparent* channel resistance of ≈ 100 Ω whereas the actual *intrinsic* value of the channel resistance is found to be ≈ 2 Ω. Therefore the sheet resistance of the channel based on RF measurements (covering approximately seven decades of the frequency range) is found to be $R_S^{RF} \approx 3.85\,\Omega/\square$, lowest measured value to date to the best of our knowledge, in contrast with $R_S^{DC} \approx 182\Omega/\square$ measured using the DC 4-probe method. This result suggests that the conventional DC 4-probe method for measuring sheet resistance may not be appropriate for single-atom thick materials such as graphene and instead our RF 4-probe method may be more accurate and reliable. Since sheet resistance, combined with the optical transparency of graphene, are the two key figures-of-merit, which are often used to optimise the production processes of graphene (in order to make quantitative comparisons with ITO which at present is the material of choice in numerous applications), it appears our proposed RF 4-probe method could make small but significant contributions in the eventual applications of graphene in solar-cells and touch-screen displays [11]. Clearly, further work is needed on a variety of other geometries and configurations of graphene 4TP impedance devices, as well as exfoliated graphene, in addition to the results reported here for CVD graphene. This would be useful towards developing a comprehensive model of the intrinsic RF electromagnetic properties of graphene, enable robust comparisons with theoretical models, and therefore may contribute to the practical applications of graphene in RF electronics, solar-cells and displays in the near future.

6. Conclusion

The RF transport electromagnetic properties of CVD graphene have been measured from DC to 110 MHz at room temperature using a calibrated precision 4TP impedance analyser. The 4TP low-frequency AC and four-terminal DC resistance of graphene are found to be approximately the same within 1 %. In general the response of the graphene 4TP impedance device was found to be strongly dependent on the quantum contact impedances at the potential leads. A lumped parameter equivalent circuit model was used to fit the measured data for apparent resistance and reactance which yielded an intrinsic, frequency independent, graphene channel resistance of R_G = 2.2 Ω or sheet resistance of $R_S^{RF} \approx 3.85\,\Omega/\square$ and contact impedance parameters of R_C = 51.6 Ω and C_C = 1.2 nF for each potential port. The intrinsic channel resistance is found to be in sharp contrast with the measured four-probe DC and 4TP low-frequency resistance value of ≈ 104 Ω or sheet resistance of $R_S^{DC} \approx 182\Omega/\square$. This suggests conventional DC sheet resistance method may not be sufficiently accurate for single-atom thick materials such as graphene, and instead our RF 4TP method may be more suitable. This could improve the accuracy and reliability of sheet resistance measurements, yielding intrinsic graphene

resistance which is free of contact influences. Furthermore, since the measured sheet resistance values are often used as a figure-of-merit for numerous applications, such as solar-cells and touch-screen displays particularly in comparison with ITO, the RF 4TP method could also impact graphene production and optimisation.

7. Acknowledgements

The authors acknowledge Dr Bryan P. Kibble, Dr David Hasko and Prof M. Z. Ahmed for useful discussions and Graphene Square Inc. for providing the graphene sample.

8. References

[1] Novoselov, K. S.; Geim, A. K.; Morozov, S. V.; Jiang, D.; Zhang, Y.; Dubonos, S. V.; Grigorieva, I. V.; Firsov, A. A. "Electric field effect in atomically thin carbon films", *Science* **2004**, 306, 666–669.

[2] Novoselov K. S.; Geim A. K.; Morozov, S. V.; Jiang, D.; Katsnelson M. I.; Grigorieva, I. V.; Dubonos, S. V.; Firsov, A. A., "Two-dimensional gas of massless Dirac fermions in graphene", *Nature **2005**, 438, 197–200.*

[3] Zhang, Y.; Tan, J. W.; Stormer, H. L.; Kim, P., "Experimental observation of the quantum Hall effect and Berry's phase in graphene", *Nature **2005**, 438, 201–204.*

[4] Castro Neto, A. H.; Peres, N. M. R.; Novoselov, K. S.; Geim, A. K., "The electronic properties of graphene", *Rev. Mod. Phys.* **2009**, 81, 109-162.

[5] Geim, A. K.; Novoselov, K. S., "The rise of grapheme", *Nature Mater.* **2007**, 6, 183–191.

[6] Balandin, A. A.; Ghosh, S.; Bao, W.; Calizo, I.; Teweldebrhan, D.; Miao F.; Lau, N., "Superior thermal conductivity of single-layer graphene", *Nano Lett.*, **2008**, 8, 902-907.

[7] Rycerz A.; Tworzydlo, J.; Beenakker, C. W. J.., "Valley filter and valley valve in graphene", *Nat. Phys*., **2007**, 3, 172-175.

[8] Xia F.; Farmer, D. B.; Lin, Y.; Avouris P., "Graphene field-effect transistors with high on/off current ratio and large transport band gap at room temperature", *Nano Lett.*, **2010**, 10, 715–718.

[9] Dean, C. R.; Young, A. F.; Meric, I.; Lee, C.; Wang, L.; Sorgenfrei, S.; Watanabe, K.; Taniguchi, T.; Kim, P.; Shepard, K. L.; Hone, J., "Boron nitride substrates for high-quality graphene electronics", *Nat. Nanotech*., **2010**, 5, 722–726.

[10] Torrisi, F.; Hasan, T.; Wu, W.; Sun, Z.; Lombardo, A.; Kulmala, T. S.; Hsieh G-W.; Jung, S.; Bonaccorso, F.; Paul, P. J.; Chu, D.; Ferrari, A. C., "Inkjet-printed graphene electronics", *ACS Nano.*, **2012**, 6, 2992-3006.

[11] Bonaccorso F., Sun, Z.; Hasan, T.; Ferrari, A. C., "Graphene photonics and optoelectronics", *Nature Photon.* **2010**, 4, 611-622.

[12] Meric, I.; Han M. Y.; Young A. F.; Ozyilmaz, B.; Kim, P.; Shepard, K. L., "Current saturation in zero-bandgap, top-gated graphene field-effect transistors", *Nature Nanotec*h., **2008**, 3, 654-659.

[13] Kedzierski, J.; Hsu, P-L.; Kong, J.; Healey P.; Wyatt, P.; Keast, C., "Graphene-on-Insulator transistors made using C on Ni chemical-vapor deposition", *IEEE Electron Dev. Lett.* **2009**, 30, 745–747.

[14] Basu, D.; Gilbert, M. J.; Register, L. F.; Banerjee, S. K.; MacDonald, A. H., "Effect of edge roughness on electronic transport in graphene nanoribbon channel metal-oxide-semiconductor field-effect transistors", *Appl. Phys. Lett.* **2008**, 92, 042114.

[15] Schwierz F., "Graphene transistors", *Nat. Nanotech.*, **2010**, 5, 487-496.

[16] Liu, M.; Yin, X.; Ulin-Avila, E.; Geng, B.; Zentgraf, T.; Ju, L.; Wang, F.; Zhang, X., "A graphene-based broadband optical modulator", *Nature* **2011**, 474, 64-67.

[17] Echtermeyer, T. J.; Britnell L.; Jasnos, P. K.; Lombardo A.; Grigorenko, A. N.; Geim, A. K.; Ferrari, A. C.; Novoselov, K. S., "Strong plasmonic enhancement of photovoltage in grapheme", *Nature Comms.* **2011**, 2, 458.

[18] Bao, Q.; Zhang, H.; Wang, B.; Ni, Z.; Lim, C. H. Y. X.; Wang, Y.; Tang, D. Y.; Loh, K. P., "Broadband graphene polarizer", *Nature Photon.* **2011**, 5, 411-415.

[19] Choi, Y-Y.; Kang, S. J.; Kim, H-K.; Choi, W. M.; Na, S-I., "Multilayer graphene films as transparent electrodes for organic photovoltaic devices", *Solar Energy Materials and Solar Cells* **2012**, 96, 281-285.

[20] Mueller, T.; Xia, F.; Avouris, P., "Graphene photodetectors for high-speed optical communications", *Nature Photon. **2010**, 4, 297-301.*

[21] Falkovsky, L. A.; Pershoguba, S. S., "Optical far-infrared properties of a graphene monolayer and multilayer", *Phys. Rev. B.* **2007**, 76, 153410.

[22] Nair, R. R.; Blake, P.; Novoselov, K. S.; Booth, T. J.; Stauber, T.; Peres, N. M. R.; Geim, A. K., "Fine structure constant defines visual transparency of graphene", *Science*, **2008**, 320, 1308.

[23] Wu, Y.; Jenkins K. A.; Valdes-Garcia, A.; Farmer, D. B.; Zhu, Y.; Bol, A. A.; Dimitrakopoulos, C.; Zhu, W.; Xia, F.; Avouris, P.; Lin, Y. M., "State-of-the-art graphene high-frequency electronics", *Nano Lett*., **2012**, 12, 3062-3067.

[24] Liao, L.; Lin, Y-C.; Bao, M.; Cheng, R.; Bai, J.; Liu, Y.; Qu, Y.; Wang, K. L.; Huang, Y.; Duan, X., "High-speed graphene transistors with a self-aligned nanowire gate", *Nature* **2010**, 467, 305−308.

[25] Lin, Y-M.; Jenkins K. A.; Valdes-Garcia, A.; Small, J. P.; Farmer, D. B.; Avouris, P., "Operation of graphene transistors at gigahertz frequencies", *Nano Lett.* **2009**, 9, 422–426.

[26] Lemme, M. C.; Echtermeyer, T. J.; Baus, M.; Kurz, H., "A graphene field-effect device", *IEEE Electron Dev. Lett.* **2007**, 28**,** 282–284.

[27] Das, S.; Appenzeller,"An all-graphene radio frequency low noise amplifier", J. *Proc. IEEE RFIC* **2011**, 1-4.

[28] Wang, H.; Hsu, A.; Wu, J.; Kong, J.; Palacois, T., "Graphene-based ambipolar RF mixers", *IEEE Electron Dev. Lett.* **2010**, 31, 906-908.

[29] Yang, X.; Liu, G.; Balandin A. A.; Mohanram, K., "Triple-mode single-transistor graphene amplifier and its applications", *ACS Nano* **2010**, 4, 5532-5538.
[30] Moon, S.; Jung, K.; Park, K.; Kim, H. J.; Lee, C-W; Baik, C-W.; Kim, J. M., "Intrinsic high-frequency characteristics of graphene layers", *New J. Phys.* **2010**, 12, 113031.
[31] Kim, W. K.; Jung, Y. M.; Cho, J. H.; Kang, J. Y.; Oh, J. Y.; Kang, H.; Lee, H-J.; Kim, J-H.; Lee, S.; Shin, H. J.; Choi, J. Y.; Lee, S. Y.; Kim, Y. C.; Han, I. T.; Kim, J. M.; Yook, J-G.; Baik S.; Jun, S. C., "Radio-frequency characteristics of grapheme oxide", *Appl. Phys. Lett.* **2010**, 97, 193103.
[32] Skulason, H. S.; Nguyen, H. V.; Guermoune, A.; Sridharan, V.; Siaj, M.; Caloz, C.; Szkopek, T., "110 GHz measurement of large-area graphene integrated in low-loss microwave structures ", *Appl. Phys. Lett.* **2011**, 99, 153504.
[33] Lee, H-J.; Kim, E.; Yook, J-G.; Jung, J., "Intrinsic characteristics of transmission line of graphenes at microwave frequencies", *Appl. Phys. Lett.* **2012**, 100, 223102.
[34] Lin, Y-M.; Dimitrakopoulos, C.; Jenkins, K. A.; Farmer, D. B.; Chiu, H-Y.; Grill, A.; Avouris, P.; "100 GHz transistors from wafer-scale epitaxial graphene", *Science* **2010**, 327**,** 662.
[35] Wu, Y.; Lin, Y-M.; Bol, A. A.; Jenkins, K. A.; Xia, F.; Farmer, D. B.; Zhu, Y.; Avouris, P., "High-frequency, scaled graphene transistors on diamond-like carbon", *Nature* **2011**, 472, 74-78.
[36] Pallecchi, E.; Benz, C. Betz, A. C.; Lohneysen, H. v.; Placais, B.; Danneau, R., "Graphene microwave transistors on sapphire substrates", *Appl. Phys. Lett* **2011**, 99, 113502.
[37] Moon, J. S.; Curtis, D.; Hu, M.; Wong, D.; McGuire, C.; Campbell, P. M.; Jernigan, G.; Tedesco, J. L.; VanMil, B.; Myers-Ward, R.; Eddy Jr., C.; Gaskill, D. K., "Epitaxial-graphene RF field-effect transistors on Si-face 6H-SiC substrates", *IEEE Electron Dev. Lett.* **2009**, 30, 650–652.
[38] Awan, S. A., Lombardo A., Colli A., Fasoli A., Echtermeyer T. J., Kulmala T. and Ferrari A. C., "Graphene Coplanar Waveguides", NT-11:Graphene Technology Satellite Meeting, Abstract p. 591, University of Cambridge, UK, 10-16th July, 2011.
[39] Rutherglen, C.; Burke P., "Nanotube electronics for radiofrequency applications", *Small* **2009**, 5, 884-906.
[40] Awan S. A. and Kibble B. P., "Towards accurate measurement of the frequency dependence of capacitance and resistance standards up to 10 MHz", *IEEE Trans. Instum. Meas.*, **2005**, 54 (2), 516-520.
[41] Callegaro L and Durbiano F, "Four-terminal-pair impedances and scattering parameters", *Meas. Sci. Technol.* **2003**, 14**,** 1–7.
[42] Awan S. A., Jones R. G. and Kibble B. P., "Evaluation of coaxial bridge systems for accurate determination of the SI farad from the DC quantum Hall effect", *Metrologia*, **2003**, 40 (5), 264-270.
[43] Awan, S. A.; Kibble, B. P.; Schurr, J., "Coaxial electrical circuits for interference-free measurements", *Book*, Publisher *IET*, 2011.
[44] Valdes, L. B., "Resistivity measurements on germanium for transistors", *Proc. IRE*, **1954**, 42, 420-427.
[45] Ferrari, A. C., Meyer, J. C., Scardaci, V., Casiraghi, C., Lazzeri, M., Mauri, F., Piscanec, S., Jiang, D., Novoselov, K. S., Roth, S. and Geim, A. K., "Raman Spectrum of Graphene and Graphene Layers", *Phys. Rev. Lett.* **2006**, 97, 187401.
[46] Cutkosky, R. D., "Four-terminal-pair networks as precision admittance and impedance standards", *IEEE Trans. Commun. Electron.* **1964**, 83**,** 19–22.